Geomorphology 163–164 (2012) 99–109

Contents lists available at Sciverse ScienceDirect

Geomorphology

journal homepage: www.elsevier.com/locate/geomorph

Modelling the equilibrium bed topography of submarine meanders that exhibit reversed secondary flows

Stephen E. Darby [a,*], Jeff Peakall [b]

[a] School of Geography, University of Southampton, Highfield, Southampton SO17 1BJ, UK
[b] School of Earth and Environment, University of Leeds, Leeds LS2 9JT, UK

ARTICLE INFO

Article history:
Received 12 July 2010
Received in revised form 11 March 2011
Accepted 12 April 2011
Available online 5 August 2011

Keywords:
Submarine channel
Bends
Meanders
Bed topography
Turbidity currents
Helical flow

ABSTRACT

Submarine meandering channels formed by turbidity currents are common; however, their location on the ocean floor and their inactive status make it difficult to measure process dynamics and bed morphology. Conceptual models have, therefore, instead been developed by analogy with the well understood mechanics of fluvial bends. However, unlike fluvial currents, in turbidity currents the downstream velocity maximum typically occurs near the bed and recent experimental and theoretical studies suggest that, under certain hydraulic and morphological conditions, this forces the secondary flow to exhibit the reverse sense to that encountered in fluvial bends. Herein the possible morphological implications of a reversal of secondary flow are explored by modelling the force balance on sediment grains moving through either (i) field and laboratory submarine meander bends that are known to exhibit 'reversed' secondary flows, or (ii) inactive submarine meander bends where the nature of the secondary flow in the formative turbidity currents can be inferred to be reversed. Exploratory simulations are undertaken for a single hypothetical submarine bend with morphological properties based on nine relic meanders observed on the floor of the Gulf of Alaska. Reconstructions of secondary flow properties within the Gulf of Alaska bends indicate that they likely exhibited reversed secondary flows. Results of the exploratory simulations indicate that, unlike typical fluvial meanders, the transverse bed profile gradient of the hypothetical bend is very low and the point bar is located downstream of the bend apex.

1. Introduction

Sinuous submarine channels primarily formed by turbidity currents are common features of the ocean floor (e.g. Damuth and Flood, 1984; Bouma et al., 1985; Kenyon et al., 1995; Clark and Pickering, 1996; Droz et al., 1996; Wynn et al., 2007). They are significant conduits for the transfer of terrestrial and shelf-derived sediment to the deep-sea and form the distributive networks of submarine fans, the largest sedimentary deposits on Earth (Curray et al., 2003). Hydrographic surveys have revealed their planform morphology, but their deep water location limits the availability of high-resolution bed topography and grain-size data. Similarly, the infrequent and destructive nature of flows through these channels inhibits detailed direct flow measurement (e.g., Khripounoff et al., 2003; Vangriesheim et al., 2009), with the most complete data to date coming from associated submarine canyons (e.g., Paull et al., 2003; Xu et al., 2004).

In lieu of detailed data, conceptual models have been developed by analogy with the well understood fluid mechanics of sub-aerial (i.e., fluvial) meander bends, on the basis that the planform morphology of submarine and fluvial meanders scales consistently (e.g., Klaucke and Hesse, 1996; Pirmez and Imran, 2003). However, recent empirical and theoretical investigations suggest that this is not always appropriate. Laboratory models of submarine channels have documented that, depending on flow parameters and/or channel geometry, submarine channel (i.e., turbidity current) flows may either show a reversed sense of helical/secondary flow to river channels (Corney et al., 2006, 2008; Keevil et al., 2006, 2007; Peakall et al., 2007a; Amos et al., 2010), or a pattern with the same orientation as river channels (Imran et al., 2007; Islam et al., 2008; Islam and Imran, 2008). Studies based on analytical and Computational Fluid Dynamics (CFD) modelling have shown that a primary control on the direction of helicity is the downstream velocity profile, in particular the height of the downstream velocity maximum above the bed (Corney et al., 2006, 2008; Giorgio Serchi et al., 2011), although factors such as cross-sectional geometry also significantly influence flow processes (Islam et al., 2008; Straub et al., 2008). Unlike fluvial currents, where the relative elevation of the maximum downstream velocity is located near the surface, gravity currents are generally considered to exhibit near-bed velocity maximums (e.g., Tesaker, 1969; Stacey and Bowen, 1988;

* Corresponding author.
E-mail addresses: S.E.Darby@soton.ac.uk (S.E. Darby), j.peakall@see.leeds.ac.uk (J. Peakall).

0169-555X © 2011 Elsevier B.V. Open access under CC BY license.
doi:10.1016/j.geomorph.2011.04.050

Garcia and Parker, 1993; Buckee et al., 2001; Felix, 2002, 2004). This has led previous workers to suggest that reversed helical/secondary circulation will dominate relative to river-like circulation (e.g., Peakall et al., 2007a; Wynn et al., 2007; Corney et al., 2008).

Abad et al. (2011) have recently attempted to cast further light on the debate concerning the fundamental fluid mechanical controls on the helicity of secondary flows in submarine channels. In their study Abad et al. (2011) extended the Corney et al. (2006) analysis to include the effects of density stratification, by considering the distance above the bed (ζ_c) below which the fractional excess density is constant. Since ζ_c affects the transverse pressure gradient, specific combinations of ζ_c and the relative height of the downstream velocity maximum (ζ_p; which affects the position in the vertical profile at which the outwards directed centrifugal force is maximized), will determine the local imbalance between the (inwards directed) pressure gradient force and (outwards) centrifugal force and thus the helicity of the secondary circulation. Abad et al. (2011) used empirical structure functions (based on 74 experimental saline density and turbidity currents) developed by Sequeiros et al. (2010) to link the parameters ζ_p and ζ_c to the densimetric Froude number ($Fr_d = \frac{U}{\sqrt{g\frac{\Delta\rho}{\rho_a}H}}$, where U is the layer-averaged flow velocity, g is the gravitational acceleration, H is the depth of the flow, and $\Delta\rho = \rho_t - \rho_a$ is the difference in density between the layer-averaged density of the current (ρ_t) and the density of the ambient fluid, (ρ_a). This enabled Abad et al. (2011) to develop a phase diagram (Fig. 1) predicting the specific hydraulic conditions that favour the onset of normal or reversed secondary flows in meandering gravity currents. The results indicate that low Froude number gravity flows promote secondary circulations that are more akin to those encountered in fluvial meander bends (since low Froude number gravity flows exhibit higher positions of both ζ_p and ζ_c, see Sequeiros et al., 2010), with reversed secondary flow circulations favoured in environments that either promote supercritical flow, or in environments with low roughness (this being expressed through the 'smoothness' parameter $C_z = 1/\sqrt{C_f}$ where C_f is the Chezy friction coefficient) and/or high velocity flows (Fig. 1).

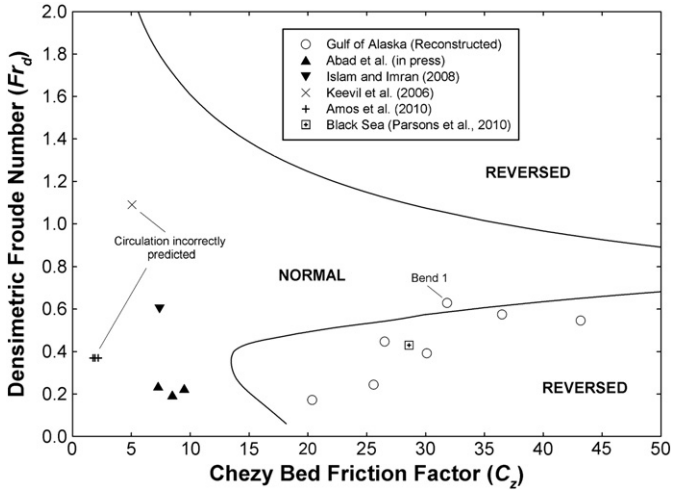

Fig. 1. Phase diagram indicating the hydraulic conditions in submarine gravity currents that favour the development of secondary flows with 'normal' and 'reversed' helicity relative to typical fluvial meander bends (from Abad et al., 2011). Estimated values of the densimetric Froude number (Fr_d) and dimensionless Chezy bed friction coefficient ($C_z = U/U_{*b}$ where U is the layer-averaged flow velocity and U_{*b} is the shear velocity at the bed) for the (inactive) Gulf of Alaska meanders investigated in this study are highlighted (open circles). The plot also shows data points for laboratory (Keevil et al., 2006; Amos et al., 2010) and field (Parsons et al., 2010) studies of density currents with known reversed secondary circulations, as well as laboratory studies of density currents exhibiting normal (river-like) secondary circulations (Abad et al., 2011; Islam and Imran, 2008).

By including the limited available data from laboratory (Keevil et al., 2006; Islam and Imran, 2008; Amos et al., 2010; Abad et al., in press) and field (Parsons et al., 2010) investigations of density currents for which the sense of the secondary circulation is in fact known, it is possible to undertake a crude validation of the Abad et al. (2011) phase diagram (Fig. 1). Depending on whether or not the Amos et al. (2010) and Abad et al. (in press) measurements are counted as either three or one separate data points on this plot, it is apparent that only 5 out of 9, or 3 out of 5, of the data points on the diagram are correctly predicted. The analysis fails to predict the reversed nature of the circulations observed in the laboratory studies of Keevil et al. (2006) and Amos et al. (2010), though as discussed by Abad et al. (2011) this may be related to the anomalously smooth nature of the channel beds employed in those studies. Moreover, the secondary circulation of the only field-scale system included in Fig. 1, the Black Sea channel observed by Parsons et al. (2010), is correctly predicted to be reversed by the Abad et al. (2011) analysis. Overall, the available data lend only equivocal support to the Abad et al. (2011) analysis. Nevertheless it is apparent from their theoretical analysis that, depending on the environmental conditions, submarine channels can exhibit either river-like or river-reversed secondary flow (Corney et al., 2008; Abad et al., in press; Giorgio Serchi et al., 2011). What is not disputed is that secondary flow imparts a strong influence on the bed morphology of, and patterns of grain-sorting in, meander bends, with a range of classical studies (e.g., Engelund, 1974; Parker and Andrews, 1985; Bridge, 1992) having documented these effects in fluvial meander bends. However, given the physical differences in the velocity structure of turbidity currents and rivers, and the impact this may have in respect of the potential reversal of the direction of helical/secondary flow in turbidity currents, this raises the question: Is the bed topography of submarine meanders different from that in fluvial streams, particularly in instances where the secondary circulation is reversed?

In this paper we undertake an assessment of the possible effects on the bed morphology of submarine meanders of reversed helical/secondary flows in turbidity currents. Our approach is to develop an idealized numerical model of bed topography for submarine meanders, concentrating on the specific case where secondary flow is reversed. The model is then used to undertake simple exploratory simulations that compare the bed morphologies of equivalent bends subjected to open-channel (fluvial) and turbidity current (reversed helicity) flows. Since the model is idealized, we view the results of these comparisons as providing preliminary insights into the possible differences in bed morphology of submarine versus fluvial meanders that arise as a consequence of the special case of secondary flow reversal. However, we also assess the predictive ability of the idealized model by comparing simulated and observed bed topographies within a total of 11 meander bends which are either: (i) formed by active gravity current flows which are *known* to exhibit reversed secondary flows (using field data from the Black Sea and from laboratory experiments), or; (ii) inactive meander bends (using field data from the ocean floor within the Gulf of Alaska) for which the sense of helicity of secondary flows within the former turbidity currents assumed to be responsible for their formation is unknown, but is inferred to be reversed based on reconstruction of flow properties within these bends. As discussed further below (see Section 3), the relative success of the model in replicating observed bed topography lends confidence in its use under this restricted range of conditions, despite its simplicity.

2. Model description

Bed topography in fluvial meanders (e.g. Engelund, 1974; Parker and Andrews, 1985; Bridge, 1992) can be modelled by solving the force balance on grains moving through the bend. Herein one of these

existing models (Bridge, 1992) is modified by replacing the logarithmic vertical profile of downstream flow velocity (as used in studies of fluvial bends) with a downstream flow velocity profile that is more appropriate for turbidity currents.

The force balance on a moving bed load grain in the *s*–*n* plane is (Bridge, 1992):

$$F_{Ds} = \mu\left(W_g - F_L\right) \tag{1a}$$

$$F_{Ds}\tan\delta^* + W_g\tan\alpha = \mu\left(W_g - F_L\right)\tan\psi, \tag{1b}$$

where F_D is the drag force, F_L is the lift force, W_g is the immersed grain weight, μ is a coefficient to account for friction between the bed and the grain, δ^* is the angle between the resultant drag force on the grain (F_D) and the downstream (s) direction ($\tan\delta^* = F_{Dn}/F_{Ds}$), α is the local transverse bed slope, ψ is the angle between the bed load grain path and the downstream direction ($\tan\psi = i_n/i_s$, where i is the volumetric unit bed load transport rate), and the subscripts s and n denote the streamwise and transverse directions, respectively. The bed topography is, therefore, obtained by solving Eqs. (1a) and (1b) for α at a series of nodes within a bend. This is achieved by developing submodels for the vertical profiles of downstream and transverse flow velocity, thereby estimating the lift and drag forces, the downstream and transverse bed load fluxes, and the angles δ^* and ψ.

Bridge (1992) used expressions for the fluid lift force derived by Bridge and Bennett (1992) to rewrite Eq. (1a) and (1b) as follows:

$$U_{bs} - V_s = V_z\left\{\mu\left[1-\left(\frac{BU_{*c}}{V_z}\right)^2\right]\right\}^{1/2} \tag{2a}$$

$$\tan\psi = \tan\delta + \frac{\tan\alpha}{E} \tag{2b}$$

where U_{bs} is the downstream flow velocity at the mean level of the bed load grains, V_s is the downstream bed load grain velocity, V_z is the terminal settling velocity estimated using the model of Dietrich (1982), B is a coefficient of turbulence anisotropy (see Bridge and Bennett, 1992), U_{*c} is the critical shear velocity, and E is given by:

$$E = \left\{\mu_c\left[1-\left(\frac{BU_{*c}}{V_z}\right)^2\right]\right\}^{1/2}\left\{\mu\left[1-\left(\frac{BU_*}{V_z}\right)^2\right]\right\}^{1/2} \tag{3}$$

where μ_c is the static friction between the bed and grain, and U_* is the shear velocity.

Note that the angle δ in Eq. (2b) is distinct from the angle δ^* in (1b). Calculation of $\tan\delta$ in Eq. (2b) requires definition of the s and n components of flow velocity at the bed (since $\tan\delta = U_{bn}/U_{bs}$), whereas δ^* is the angle between the resultant drag force on the grain (F_D) and the downstream (s) direction. However, the modelling procedure is iterative, meaning that initial estimates of $\tan\delta$ and the initial bed topography are required. Full details of the method used to provide this initial estimate of bed topography are provided in Bridge (1992), and they are not repeated here for reasons of clarity. Suffice to say that the method of Engelund (1974) is employed in which the bed topography is forced by variations in radius of curvature along a sine-generated curve.

Regarding the initial value of $\tan\delta$, this is estimated based on the method of Kikkawa et al. (1976) in which the primary and secondary flow velocities are calculated for steady, uniform curved flows. The Kikkawa et al. (1976) method assumes that the governing flow momentum equations can be simplified by (i) ignoring vertical components of flow velocity, (ii) assuming that partial derivatives with respect to the local radius of curvature (r) are small compared to those with respect to z, and (iii) the transverse flow velocity components are small relative to the primary flow velocity components. Such conditions are normally satisfied in the case of wide channels with a large radius of curvature (Bridge, 1992). Using the Kikkawa et al. method, Bridge (1992) writes that the vertical distribution of transverse velocity is given by:

$$\frac{U_n}{\bar{U}_{so}} = \left(\frac{\bar{U}_s}{\bar{U}_{so}}\right)^2\frac{d}{r}\frac{1}{\kappa}\left[F_1\left(\frac{z}{d}\right) - \frac{1}{\kappa}\frac{U_{*o}}{\bar{U}_{so}}F_2\left(\frac{z}{d}\right)\right] \tag{4}$$

where κ is the Von Karman constant, d is the flow depth, r is the bend radius of curvature, $\bar{U}_s$ is the depth-averaged downstream velocity, and the subscript o denotes quantities at the channel centre line. When the functions F_1 and F_2 are evaluated at the bed, Eq. (4) gives (Bridge, 1992):

$$\frac{U_{bn}}{\bar{U}_{so}} = \left(\frac{\bar{U}_s}{\bar{U}_{so}}\right)^2\frac{d}{r}\frac{1}{\kappa}\left[\frac{1}{\kappa}\frac{U_{*o}}{\bar{U}_{so}}2.64 - 4.17\right]. \tag{5}$$

Bridge (1992) used a logarithmic vertical flow profile appropriate for hydrodynamically rough open channels (see below for further discussion of this assumption) to determine the necessary near-bed value of U_s, eventually yielding the following formula which is used to estimate the initial value of $\tan\delta$:

$$\tan\delta = \frac{U_{bn}}{U_{bs}} = \frac{\bar{U}_s}{\bar{U}_{so}}\frac{d}{r}\frac{1}{8.5\kappa}\left[\frac{2.64}{\kappa} - 4.17\frac{U_{so}}{U_{*o}}\right]. \tag{6}$$

It is important to note that Eq. (5) describes the transverse flow distribution in both open-channel and gravity current flows (see Corney et al., 2006; though note that strictly Eq. (5) as applied by Corney et al. is for low curvature bends), the transverse flow being forced by values of the downstream flow velocity ($\bar{U}_{so}$, $\bar{U}_s$, and U_{*o}) and bend morphology (represented here in terms of the flow depth, d, and bend radius of curvature, r) parameters that are appropriate for a specific application. However, the significance of this point in respect of applications to submarine meanders is as follows. In his model for fluvial channels, Bridge (1992) estimated the near-bed value of U_s using a logarithmic law-of-the-wall for hydraulically rough flows, which yields:

$$\tan\delta = \frac{U_{bn}}{U_{bs}} = A\frac{d}{r} \tag{7}$$

where A is given by (Bridge, 1992):

$$A = \frac{1}{8.5\kappa}\left[\frac{2.64}{\kappa} - 4.17\frac{\bar{U}_{so}}{U_{*o}}\right]. \tag{8}$$

As with Eq. (5), Eqs. (6) to (8) can be used to estimate $\tan\delta$ in Eq. (2b), so long as suitable values of U_{so} and U_{*o} are used. However, for gravity currents numerous studies (e.g., Stacey and Bowen, 1988; Altinakar et al., 1996; Felix, 2002; Xu et al., 2004; Corney et al., 2006; Keevil et al., 2006; Xu, 2010) have shown that the downstream flow velocity profile is not a logarithmic function of distance from the boundary, but instead can be described using:

$$\frac{U_s}{U_{s\,max}} = 10\left(1-\frac{z}{H}\right)^3\frac{z}{H} \tag{9}$$

where U_{smax} is the maximum downstream velocity, and H is the thickness of the flow. However, normalizing (9) with U_{smax} is unhelpful as the latter is unknown *a priori*. An alternative form in which U_s is normalized by the shear velocity, U_*, gives:

$$\frac{U_s}{U_*} = K\left(1-\frac{z}{H}\right)^3\frac{z}{H} \tag{10}$$

where $K = 10U_{smax}/U_*$, and the shear velocity is estimated using (Kneller, 2003):

$$U_* = \sqrt{g\frac{\Delta\rho}{\rho_a}HS} \tag{11}$$

in which the excess density $\Delta\rho = \rho_t - \rho_a$, with ρ_t the density of the turbidity current fluid and ρ_a the density of the ambient fluid, respectively, and S is the local channel gradient measured along the thalweg. Note that the ratio $\Delta\rho/\rho_a$ is the layer-averaged fractional excess density. From Eqs. (9) and (10), the depth-averaged velocity, $\overline{U}_s$, is readily obtained.

Fig. 2 indicates that the shape of the downstream flow velocity profile for gravity currents as modelled using Eq. (10) is such that the velocity maximum is near the bed, not at the surface as would be the case for the logarithmic function used in the original Bridge (1992) formulation for open-channel values. For this reason Eqs. (5) to (8), and therefore the pattern of secondary flow, are entirely determined by the logarithmic streamwise velocity functions employed by Kikkawa et al. (1976), and subsequently utilized by Bridge (1992), and so do not generally hold for the gravity current velocity profile represented by Eq. (10). This means that the model presented is not valid for predictions aimed at resolving the vertical variation of the transverse flow field. Nevertheless, we argue that the values of U_* and $\overline{U}_s$ as obtained from Eqs. (10) and (11) in conjunction with an estimate of the value of the parameter K (see below), can be substituted into Eqs. (5) to (8) for the purposes of solving for tan δ and resolving the grain force balance *at the bed*. This is because the flow velocity profile for gravity currents as described by Eq. (10) and the original logarithmic functions differ by only a small degree in the region of the flow immediately above the bed. For the same reason, other factors that are neglected in the above formulation, such as the effects of drag on the upper surface of the gravity flow, may be assumed to have a relatively minor impact on the forces acting on sediment grains at the bed.

As noted above, to close the model it is necessary to provide an estimate of the parameter K. Unfortunately, very few studies have been published that report all the data necessary to estimate K. Exceptions include the direct measurements of turbidity currents in Monterey Canyon and Hueneme Canyon undertaken by Xu et al. (2004) and Xu (2010), respectively, whose data yield $1.12 < K < 3.54$, and the experimental studies of Corney et al. (2006), Keevil et al. (2006) and Amos et al. (2010), all of which employed saline density flows and for which $K = 4.69$, 7.21 and 4.32, respectively. It is therefore tentatively suggested that a conservative range of $1 < K < 10$ might encompass most natural turbidity currents, while noting that the lack of data means that K is not yet well constrained. As such the effects of uncertainty in the parameterization of K on bed topography predictions are explored later (see Section 4 and Fig. 5). Fig. 2 shows that the physical effect of increasing K is to enhance the strength of the vertical gradient of downstream flow velocity (i.e., increasing K increases the boundary shear stress), but that the location of the velocity maximum within the vertical is unaffected. Consequently, in the simulations reported in this study the resulting transverse velocities show a reversed secondary circulation relative to rivers for all K values, in agreement with the theoretical and experimental results of Corney et al. (2006, 2008) and Keevil et al. (2006, 2007). The secondary circulation observed and predicted by Corney et al. (2006, 2008) and Keevil et al. (2006, 2007) and reproduced herein differs from some other recent gravity current experiments (e.g., Islam and Imran, 2008; Islam et al., 2008), most likely as a result of the relative height of the velocity maximum (see Corney et al., 2008) and the nature of the bend geometry, as discussed in Section 1.

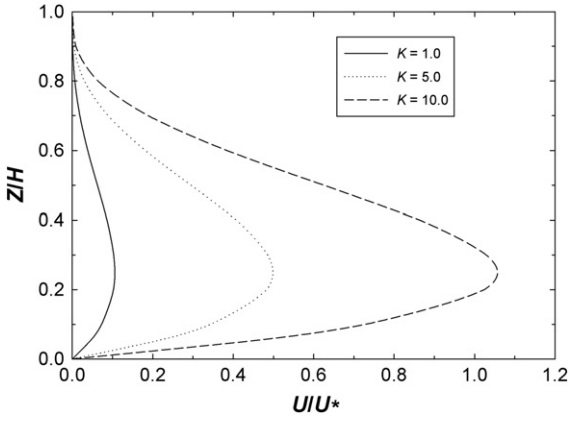

Fig. 2. Influence of the parameter K on the vertical profile of downstream flow velocity as modelled using Eq. (10). Note that Z is the local flow depth, H is the thickness of the flow, U is the downstream flow velocity and U_* is the shear velocity.

The above provides a quantitative basis for understanding how differences in the 'river-like' secondary flow circulation of typical open-channel flow meanders and the 'reversed' circulation associated with some gravity currents potentially lead to differences in the bed topography of these distinctive geophysical flows. Specifically, such differences in simulated bed topography can be understood to be forced by any differences in the numerical values of the key parameters that comprise the force balance expressed in Eqs. (1) and (2). We discuss this further in Section 4, but it can be noted here that the immersed grain weight (W_g), and bed friction coefficient (μ) are unlikely to differ significantly in open-channel versus gravity current flows. Furthermore, differences between gravity current and open-channel flows in the fluid lift force (F_L) exerted on grains are also likely negligible for the reason cited above, namely that the differences in vertical velocity profiles described by Eqs. (10) and the logarithmic law-of-the-wall for gravity currents and open-channel flows, respectively, are minor in the near-bed region relevant to the force balance on grains. Consequently, variations in the transverse bed profiles of gravity current flows with reversed secondary flows and typical open-channel flow meanders as modelled herein can be understood to be forced by variations in the drag force on the grain (F_{Ds}; with increases in the drag force causing reductions in the transverse bed gradient), the parameter tan δ^* (with increases in tan δ^* leading to a reduced transverse bed gradient), and tan ψ (with increases in tan ψ leading to steeper transverse bed profiles).

It is also worthwhile re-iterating that we accept that the above model is an idealized representation of flow and sedimentation processes within submarine meander bends shaped by turbidity currents. It is important to recognize that not only are important elements of the physics of these processes simplified (e.g. higher order terms in the governing flow momentum equations are assumed negligible, cross-channel variations in stratification are neglected), but that consequently the model as developed is valid for a specific range of submarine meander channels. Specifically, the model presented here is intended for use in exploratory simulations of submarine meander morphology in systems: (i) that exhibit a reversed secondary circulation forced by relatively low heights of the downstream flow velocity maximum above the bed; (ii) that are dominated by bed load sediment transport; (iii) wherein cross-channel variations of stratification at the bed are negligible, and (iv) which meet the assumptions implicit in the Bridge (1992) model derivation (channel planform according to a sine-generated curve, low radius of curvature bends, channels with high width to depth ratios, etc).

3. Assessment of model performance

While accepting that the above developed model is both idealized and restricted to specific classes of submarine meander bends that exhibit reversed secondary flow, it is nevertheless important to be assured that its predictions are accurate. Therefore we now assess the predictive capabilities of the model by comparing predicted and observed transverse bed profiles at the apices of meander bends shaped by turbidity currents. A total of three data sets are used, comprising gravity current flows which exhibit reversed secondary flows using (i) field data from an active submarine channel bend in

Table 1
Parameter values used in the model simulations. GoA denotes the Gulf of Alaska study bends, the numeral corresponding to the individual bends shown in Fig. 3. Symbols: W = channel width, λ = channel wavelength, R/W = ratio of radius of curvature to channel width, H = flow depth, W/H = width to depth ratio, S = channel gradient, ρ_t = layer-averaged density of gravity current flow, and ρ_a = density of ambient fluid.

Bend	W (m)	λ (m)	R/W	H (m)	W/H	S	ρ_t (kg/m^3)	ρ_a (kg/m^3)
Validation simulations								
Black Sea	850	18,000	9.4	20.0	42.5	2.00×10^{-4}	1027	1013
Amos et al. 40°	0.12	0.869	1.5	0.05	2.4	4.60×10^{-2}	1025	1000
Amos et al. 60°	0.12	1.035	1.2	0.05	2.4	3.87×10^{-2}	1025	1000
Amos et al. 80°	0.12	1.363	1.2	0.05	2.4	2.94×10^{-2}	1025	1000
GoA 1	650	60,590	23.4	120.5	5.4	4.00×10^{-4}	1055	1030
GoA 2	2730	32,350	3.2	126.4	21.6	2.91×10^{-4}	1055	1030
GoA 3	2570	26,160	3.0	173.3	14.8	1.73×10^{-4}	1055	1030
GoA 4	1420	28,080	5.0	140.4	10.1	2.54×10^{-4}	1055	1030
GoA 5	1110	21,160	6.3	145.9	7.6	1.64×10^{-4}	1055	1030
GoA 6	1330	25,540	4.5	219.9	6.0	9.30×10^{-5}	1055	1030
GoA 7	950	33,100	6.0	288.6	3.3	7.27×10^{-5}	1055	1030
Model sensitivity test								
SM1 and FM1	1540	32,400	7.3	173.6	8.9	3.26×10^{-3}	1025	1000

Note that the following physical constants were employed in all the simulations: Von Karman constant (κ) = 0.04, kinematic viscosity (υ) = 1.0×10^{-6} m^2/s, sediment suspension criterion (B) = 0.8, sediment density (ρ_s) = 2650 kg/m^3, dynamic (μ = 0.6) and static (μ_c = 0.6) grain resistance coefficients, and p in bed load transport equation = 3.0. Note also that the flow depth (H) used in these simulations is equated to the mean depth below the levee crest, see Fig. 3C. Values of the parameter K employed in the simulations were 8.72, 4.32 and 5.0 for the Black Sea, Amos et al. (2010) and Gulf of Alaska bends, respectively.

the Black Sea, (ii) three meander bends simulated in laboratory experiments and; (iii) seven inactive meander bends (using field data from the ocean floor within the Gulf of Alaska) for which the sense of helicity of secondary flows within the former turbidity currents assumed to be responsible for their formation is, therefore, unknown, but can be inferred to be reversed based on flow reconstructions (see below and Fig. 1).

The field data from the Black Sea is for a channel bend present on the SW Black Sea shelf, immediately to the north of the Bosphorus Strait (Flood et al., 2009; Parsons et al., 2010). The density difference between the hyper-saline Mediterranean and the brackish Black Sea drives exchange through the strait (Özsoy et al., 1995, 2001), resulting in a dense saline flow exiting onto the Black Sea shelf where it flows through a large channel bend before splitting into a distributary channel network (Flood et al., 2009). The channelised flows are almost continuously active, exhibit a quasi-steady discharge and, perhaps uniquely, are in long-term equilibrium with the bounding topography (Flood et al., 2009; Parsons et al., 2010). Importantly for this present study, Parsons et al. (2010) have recently obtained direct measurements of the flow structure in this channel using an RDI 600 kHz acoustic Doppler current profiler (aDcp) deployed from a Huntec towfish at a height of approximately 40 m above the sea-bed, on a series of repeat cross-sections across the bend apex (Parsons et al., 2010). Crucially, these cross-sections, once averaged and rotated to provide a zero cross-stream flux, reveal a reversed secondary circulation marked by strong outwardly directed basal flows and inwardly directed return flows higher up in the flow (Parsons et al., 2010). This, along with the presence of bedforms and mobile bars within the channel which suggests that bedload is important in this system (Flood et al., 2009; Parsons et al., 2010), confirms that the site is appropriate for use in this study. Detailed bathymetric surveys of the Black Sea channel have also been undertaken using a Kongsberg EM-3002 multibeam sonar (Flood et al., 2009), providing post-processed gridded data of the bend at a 5 m resolution in the horizontal and vertical information accurate to within <1% of water depth. These gridded data were then imported into ArcGIS9.3, with raster-based measurement tools then being used to determine the parameters required for input to the model (Table 1), and to extract a cross-section at the bend apex for comparison with model output (the bend apex cross-section data corresponding to the cross-section flow data of Parsons et al., 2010).

The three laboratory data points used in this study (Table 1) are taken from the experiments of Peakall et al. (2007a) and Amos et al. (2010), who modelled saline density currents over mobile sediment beds within bends of fixed geometry. Channel sinuosity was varied across three experiments from 1.14, through 1.36 to 1.78, with each experimental planform consisting of bends of constant radius separated by straight sections. Flow data was measured using ultrasonic Doppler velocity profiling, enabling two-dimensional flow fields to be measured (Best et al., 2001). In these experiments an array of ten 4 MHz probes recorded cross-section velocities at bend apices (Peakall et al., 2007a; Amos et al., 2010), and a similar array measured downstream velocities. Reversed secondary flows were recorded in all three experiments (Peakall et al., 2007a; Amos et al., 2010), consistent with the structure of secondary flows recorded in the same channels in the absence of sediment beds (Corney et al., 2006; Keevil et al., 2006). The mobile bed consisted of angular, polydisperse sediment of low density, enabling it to move predominantly as bedload, and develop topography over time (Amos et al., 2010). At the end of each experiment, the bed topography was measured using an ultrasonic bed profiler (Best and Ashworth, 1994) at a grid spacing of 10 mm. This data was gridded in Surfer and the bend apex cross-sections exported using the Surfer tools.

Field data from the Gulf of Alaska are derived from baythmetric surveys (Fig. 3A) undertaken by the Center for Coastal and Ocean Mapping/Joint Hydrographic Center (CCOM-JHC) at the University of New Hampshire. These surveys employed a hull-mounted Kongsberg Simrad EM120 12-kHz multibeam sonar in water depths between 1000 and 5000 m, providing gridded (100 m/pixel) data accurate to within ±0.5% of water depth (Mayer et al., 2005). These data reveal large meandering channel systems (location: ~55.5 N 137.5 W) at a depth of ~3000 m, within which seven specific study bends (Fig. 3B) with morphology broadly consistent with other submarine channels were selected for analysis. Specifically, the gridded bathymetric data were visualized in ArcGIS 9, using Arc's measurement tools to define the parameters required for input to the model (see Table 1), and to extract cross-sections at bend apices for comparison with model output.

In contrast to the Black Sea field data and the Amos et al. (2010) laboratory experiments, the turbidity currents that are assumed to have formed the Gulf of Alaska (GoA) meanders are inactive under contemporary sea-levels. As such no direct evidence is available regarding the nature of the former secondary flow circulations in these channels. However, we have employed the bathymetric data as described above to extract the necessary channel gradient, channel width, flow super-elevation (see below), and radius of curvature data

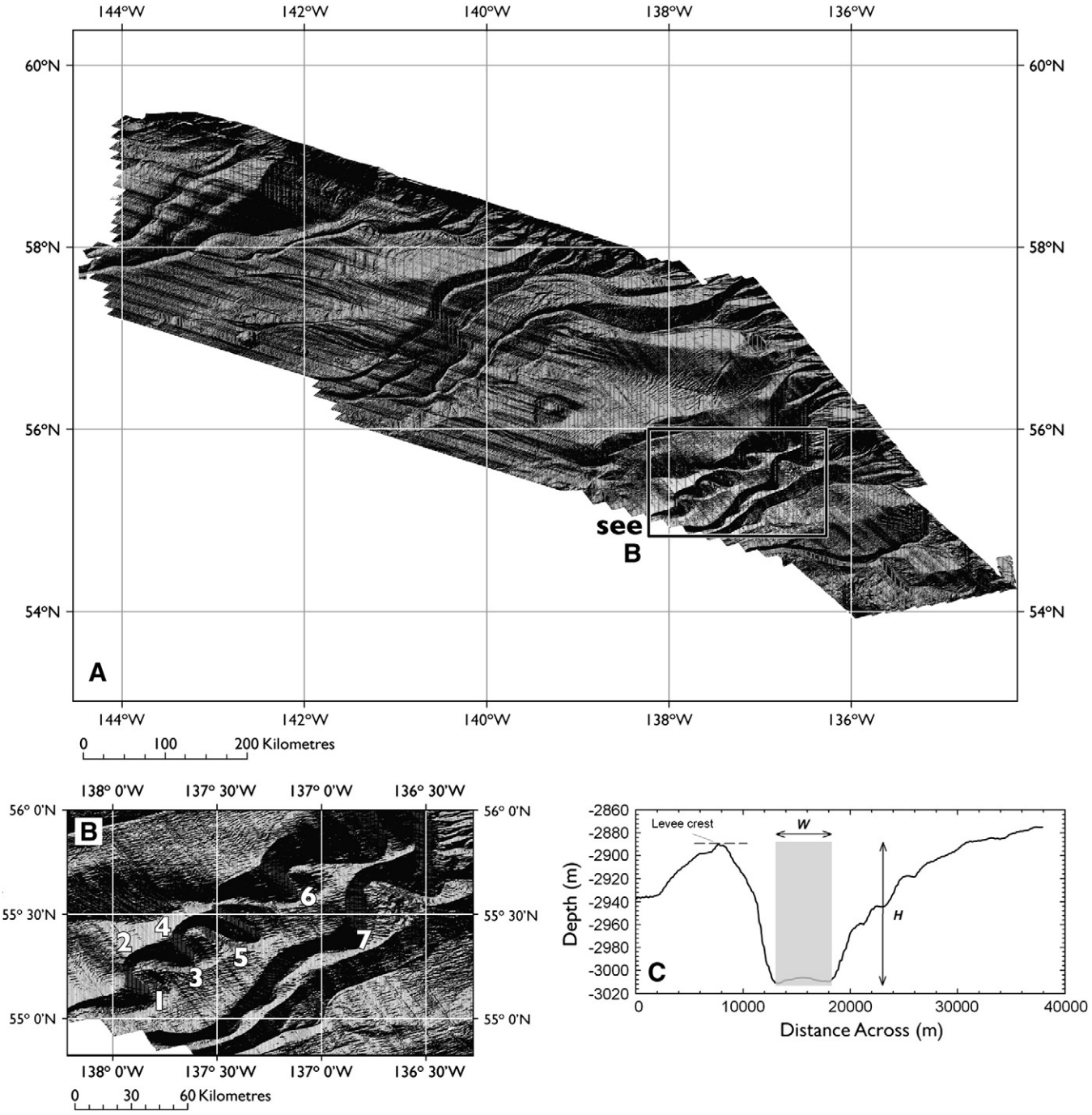

Fig. 3. (A) Hillslope shaded bathymetric survey data for the Gulf of Alaska region showing the meander system and (B) specific bends modelled in this study. Flow is from the NE to SW. (C) Cross-section showing the measurement of width (W) and channel depth (H). Note that the width employed here is the bed width, which is the distance between the toes of the two channel banks. The position of the bank toes is determined by identifying local maxima in the second derivative of the transverse side slopes. *Data from*: http://www.ccom-jhc.unh.edu/.

to support a reconstruction of flow conditions in the Gulf of Alaska channels following Pirmez and Imran (2003). Specifically, we adopt Pirmez and Imran's (2003) method of using Komar's (1969) cross-flow momentum equation to compute the former layer-averaged downstream flow velocity (U) through each channel bend:

$$\frac{\rho_t U^2}{R} = g\Delta\rho\frac{dh}{dr} \pm \rho_t f U \tag{13}$$

where R is the bend radius of curvature, dh/dr is the slope of the upper flow interface along the radial direction, r; and f is the Coriolis acceleration ($f = 2\Omega\sin\phi$, with $\phi = 55°$N for the Gulf of Alaska, and Ω is the angular speed of the Earth's rotation $= 7.3\times10^{-5}$ rad/s. Note that the Coriolis term is positive when the meander bend turns to the right and negative if it turns to the left).

In this approach, which assumes steady uniform flow, estimated (for the former current density and excess density) and measured values for R and f, enable Eq. (13) to be presented as a quadratic that can be solved for U when the remaining unknown (dh/dr) is specified. The key assumption, therefore, is that the cross-slope between the outer and inner levee across each meander bend (clearly recognizable on the Gulf of Alaska cross-sections, see Fig. 3C), can be equated to the super-elevation of the upper flow interface dh/dr (Pirmez and Imran, 2003). The estimated flow velocities obtained using this procedure fall

in the range ~1.4 to ~3.4 m/s (mean value ~2.6 m/s). Together with the measured flow depths ($\sim 120 \leq H \leq \sim 290$) and channel gradients ($7.3\times10^{-5} \leq S \leq 4.0\times10^{-4}$), these flow velocity data were used to compute the densimetric Froude numbers and Chezy bed friction coefficients. The values obtained indicate that six of the seven Gulf of Alaska meander bends (the exception is Bend 1, which plots close to the discriminating line) fall within the reversed secondary flow regime predicted by the Abad et al. (2011) phase diagram (Fig. 1), providing some degree of confidence that it is appropriate to apply the model developed herein to these data.

We emphasize that the above reconstruction of 'reversed' secondary flows in the relic Gulf of Alaska bends is fundamental to ensuring that the data used match the assumptions employed within our model. As noted previously the available data, which admittedly is limited in extent, lends only equivocal support to the use of the Abad et al. (2011) analysis for this purpose, with further uncertainties embedded within the reconstruction itself. In addition the Gulf of Alaska channels evidently exhibited sub-critical flows. The low densimetric Froude numbers of our reconstruction (Fr_d<0.6, see Fig. 1) should promote flow velocity maxima that are somewhat distant from the bed (at Z/H values of ~0.5 to 0.6) according to the laboratory data of Sequeiros et al.(2010), which is higher than the position of the flow velocity maximum of $Z/H = 0.25$ associated with Eq. (10) as employed herein. If the reconstruction undertaken above and the Abad et al. (2011) analysis are both correct, it is evident that it is the high Chezy bed roughness coefficients computed for these channels that are responsible for the modelled bends apparently conforming to the key assumption of reversed secondary flow (see Fig. 1).

To close the model it is necessary to select appropriate values of the parameter K for each of the three data sets. For the Black Sea and Amos et al. (2010) data sets values of K can be determined through direct analysis of observed downstream flow velocity profiles via Eq. (10), giving values of K of 8.72 and 4.32, respectively (Table 1). However, such flow velocity data is not available for the (inactive) Gulf of Alaska bends. For these bends simulations were therefore undertaken using a value of $K = 5.0$. This choice is arbitrary but it falls within the range of the K values obtained for the other (empirical) data sets used herein while sitting at the approximate mid point of the $1 \leq K \leq 10$ range discussed previously.

These three data sets together provide data on observed transverse bed profiles for a total of 11 meander bends, with the assessment of model performance based on determining the fit between simulated and observed transverse bed slopes (St) at the apices of the investigated bends (Fig. 4). This is consistent with previous studies in river channels (e.g., Darby and Delbono, 2002) which have focused on bend apices on the basis that this region likely experiences fully-developed secondary flow. It should be noted that comparisons of transverse bed gradient may be prejudiced if the shape of the bend morphology diverges from an approximately linear profile, but the linear profile is a reasonable approximation for all the bends simulated here. Fig. 4 illustrates that the model replicates the observed transverse bed slopes at bend apices reasonably well. To account for the uncertainties inherent in the parameterisation of K, the error bars in Fig. 4 reflect the range of simulated transverse bed gradients obtained by varying K in the range $1 \leq K \leq 10$. A linear regression (of the form $St_{pred} = c + m\,St_{obs}$) through the data points on this plot (i.e. through the data points obtained using values of $K = 8.72$, 4.32, and 5.0 for the Black Sea, Amos et al. (2010) and Gulf of Alaska bends, respectively) was used to compare observed and simulated transverse bed gradients quantitatively. The values of the gradient ($m = 2.89$) and intercept ($c = 2.3\times10^{-3}$) obtained indicate the tendency of the model to over-predict the transverse bed slope, though the value of the coefficient of determination of the regression ($r^2 = 0.777$) highlights the relatively low degree of scatter in the relationship.

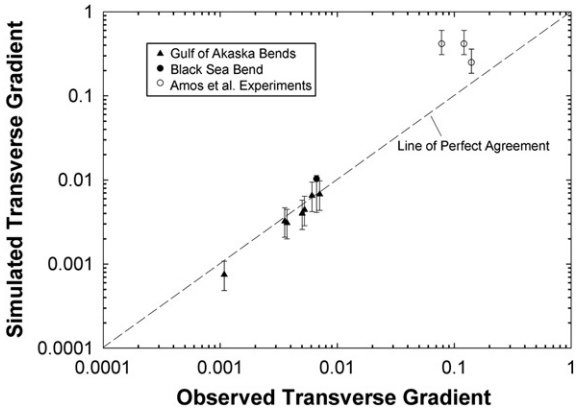

Fig. 4. Comparison of observed and simulated transverse bed gradients at the apices of: seven presently inactive submarine meander bends assumed to be formed by turbidity currents and located in the Gulf of Alaska (closed triangles, $K = 5.0$); an active submarine meander located in the Black Sea (closed square, $K = 8.72$), and; three experimental meander bends formed by the laboratory density currents of Amos et al. (2010) (open circles, $K = 4.32$). The error bars denote the transverse bed gradients obtained by varying the parameter K (see Eq. 10) in the range $1 \leq K \leq 10$. The dashed line represents the line of perfect agreement. Parameter values used in these simulations are listed in Table 1.

An additional quantitative metric of model fit is the discrepancy ratio (defined as the ratio between predicted and observed transverse bed slope, so that a discrepancy ratio of 1.0 indicates perfect fit). Discrepancy ratios for the 11 individual bends range from 0.69 to 5.35, with the overall mean discrepancy ratio of 1.62 confirming the systematic over-prediction of transverse bed slope. It is noteworthy that the data from the Amos et al. (2010) experiments plot as outliers in Fig. 4, so that the three largest discrepancy ratio values (ranging from 1.79 to 5.35) are associated with these data points. Were these three data points to be excluded, the mean discrepancy ratio for the remaining 8 bends becomes 0.91 (with the adjusted regression coefficients $m = 1.22$, $c = 1.3\times10^{-3}$ and $r^2 = 0.945$), indicating a slight tendency for model under-prediction of transverse bed slope. Possible explanations for the large model errors associated with the Amos et al. (2010) experiments include the facts that (i) the high curvature and low width to depth ratios of these bends (see Table 1) do not conform closely to the assumptions made in the model derivation (which requires infinitely wide, low curvature bends) and (ii) the fibreglass floor of their flume channel was completely smooth. It is therefore possible that the experimental cross-sections in their mobile beds were not able to support steep transverse slopes, since the bed material may fail on the underlying smooth basal surface. However, whether or not this was in fact a problem in these experiments remains unknown.

The above results provide some confidence that the model can be applied to predict the bed topography within submarine meanders, at least within bend apex sections. However, as mentioned previously it is necessary to consider whether uncertainties in parameterizing K are sufficiently high to confound the utility of the resulting model predictions. This issue is discussed further in the next section.

4. Bed topography of submarine meanders with reversed secondary flow circulations

The primary goal of this study was to explore the ways in which the bed topography of specific classes of submarine meanders may differ from, or be similar to, that of fluvial bends. In this section we explore this question by undertaking exploratory comparative simulations using (i) the modified model for submarine meanders (simulation set SM1) as presented herein, and (ii) Bridge's (1992) model for fluvial bends (simulation set FM1). Parameter sets (Table 1) for the two models are identical, with the exceptions that in FM1 the

parameter K is not used and the layer-averaged fractional excess density ($\Delta\rho/\rho_a$) is replaced with the fluid density for freshwater ($\rho = 1000$ kg/m^3). The parameter values used in these simulations are based on the mean values for the Gulf of Alaska data set. Note that, strictly speaking turbidity current density (ρ_t) and ambient fluid density (ρ_a) values of 1055 kg/m^3 and 1030 kg/m^3, respectively, are more appropriate for the oceanic turbidity currents simulated in the submarine meander scenario (SM1). These values would give a layer-averaged excess density of 0.024, but the parameter values used in Table 1 provide a very similar excess density of 2.5% while enabling a more direct comparison with the fluvial meander scenario. The excess density value of 2.5% used here is within the range of sediment concentrations expected in submarine channels (Pirmez and Imran, 2003).

In a first series of sensitivity analyses, the bend sinuosity is systematically varied to force variations in the bend radius of curvature. The results (Fig. 5) show that the resulting overall form of the expected inverse non-linear relationship between the radius of curvature to width ratio (R/W) and the transverse bed profile at the bend apex is similar for both the submarine and fluvial meander bends. Specifically, in both scenarios simulated transverse bed gradients at bend apices become more subdued as R/W increases (i.e., as bend curvature decreases). However, of particular significance in the context of the present study is that the simulated transverse bed profile gradients are significantly (by approximately an order of magnitude) lower in the simulated submarine meander bends versus equivalent fluvial bends.

Fig. 5 also illustrates that varying K from 1.0 to 10.0 results in an approximately twofold variation in the transverse slopes simulated at bend apices (similar to the range described by the error bars in Fig. 4), with the simulated transverse bed gradients becoming steeper as K increases. As such it is clear that the choice of the K value has a large influence on the specific meander bed topographies simulated in this study. While the twofold spread of simulated transverse bed profiles as a function of K shown in Fig. 5 is large, it is noteworthy that this range is insufficient to cause predictions from the submarine meander model scenarios (SM1) to overlap with the transverse bed slope predictions associated with terrestrial meanders (FM1). Put another way, variations in meander bed topography induced by uncertainties in specifying the value of K are not large enough to affect a key result of this study, namely that the reversed secondary flows associated with some turbidity currents generate submarine meander bed topographies that significantly differ from their fluvial counterparts (see below). Nor is the fact that the precise form of the imposed vertical velocity profile has a significant influence on the resulting bed topography surprising. Indeed, systematic downstream variations in submarine meander morphology have been observed in nature

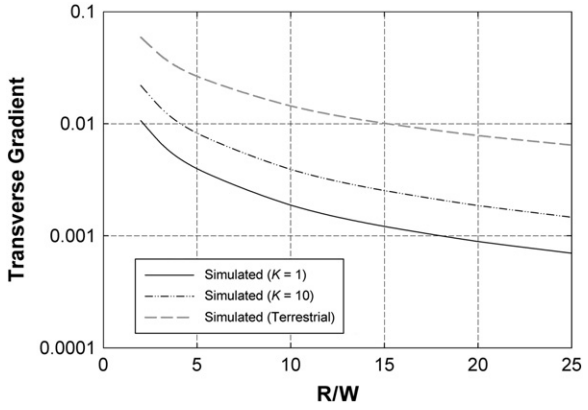

Fig. 5. Simulated relationship between transverse bed gradient at bend apices and R/W for submarine meanders (with $K = 1$; solid black line and $K = 10$; broken black line) and equivalent fluvial meanders (dashed grey line).

(Babonneau et al., 2002; Pirmez and Imran, 2003). It is possible that such variations could be interpreted in terms of the changing value of K (within the reversed flow regime) as oceanic turbidity currents evolve during their passage from shelf to abyssal plain, as an additional factor to the threshold changes between secondary flow regimes (forced by variations in Fr_d and C_z, see Fig. 1) that are likely along this environmental gradient.

In the second sensitivity test undertaken here, we explore detailed differences in bed topography within submarine versus fluvial meander bends. It should be noted that this sensitivity test should be considered exploratory in nature, being undertaken only for a single hypothetical bend with morphological properties based on those from the Gulf of Alaska data set as mentioned above. The results (Fig. 6; note that Fig. 6C is a difference map presented to illustrate the differences between the hypothetical submarine bend simulated in Fig. 6A and the equivalent fluvial meander bend in Fig. 6B) highlight that the hypothetical submarine meander bend exhibits two key differences in bed morphology relative to an equivalent fluvial bend. The first confirms the result highlighted by the sensitivity tests illustrated in Fig. 5, namely that the outer-bank pool is shallower and the 'point bar' less pronounced in the submarine meander, resulting in a transverse bed profile that, particularly at the bend apex, is very flat in relation to the equivalent fluvial bend.

As noted in Section 2, the above finding can be explained in mechanistic terms through consideration of the relative magnitude of the key terms in the force balance acting on grains in submarine (with reversed secondary flows) and fluvial meanders. Specifically, the parameters tan δ^* and tanψ are both increased in magnitude in situations where the secondary circulation has outwards directed flow near the bed, as is the case in the submarine bends simulated here. However, as noted previously, the influence of these two parameters acts in opposite directions, with increases in tan δ^* tending to reduce the transverse bed gradient and increases in tan ψ tending to increase the transverse bed gradient. The third key parameter in the force balance is the downstream drag force (F_{Ds}). It is likely that F_{Ds} is greater in submarine versus fluvial channel bends due to the relatively strong vertical velocity gradient of the former as compared to the latter. Given the counter-balancing tendencies of the parameters tan δ^* and tan ψ this would superficially suggest that it is the relatively higher values of F_{Ds} that are the dominant factor in inducing reductions in the transverse bed gradient of the submarine versus fluvial meander bends simulated herein. However, Fig. 5 shows that increasing the value of the parameter K, which should *increase* the magnitude of F_{Ds} (see Fig. 2) leads to an increase, not decrease, in the transverse bed gradient. As such a more nuanced explanation recognizes that the parameter K also influences the values of tan δ^* and tan ψ, respectively. Thus for relatively low values of K the parameter F_{Ds} provides the dominant contribution to the simulated reduction (relative to fluvial bends) in transverse bed gradient of submarine meanders, but as K increases the relative magnitude of the term tan δ^* grows at a faster rate than both F_{Ds} and tan ψ, such that tan δ^* dominates the force balance for submarine bends with higher values of K.

The second point concerns differences in the position of the point bar. Specifically, Fig. 6 shows that the point bar simulated in the case of the hypothetical submarine meander is located somewhat downstream of the bend apex position that is normally occupied by fluvial point bars. It should be noted that we are unable to explore this result for specific bends within the Gulf of Alaska dataset because the resolution of the bathymetric data is inadequate to reliably discriminate the position of the point bar (see also below), even though the transverse slope can be quantified reliably.

Although the above results are obtained using a highly idealized model and are based on a single bend, they are consistent with those from recent physical modelling studies of (i) deposition within pre-formed submarine channels (Peakall et al., 2007a; Amos et al., 2010),

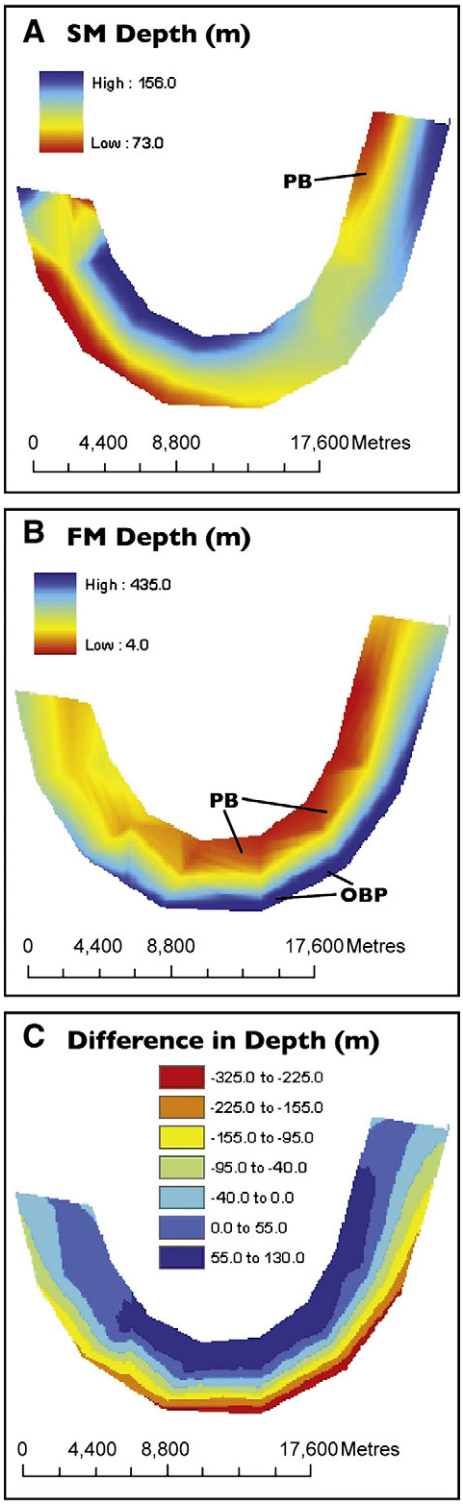

Fig. 6. Simulated bed morphology using (A; left) the submarine meander model presented in this study, (B; centre) the unmodified model by Bridge (1992) for subaerial meanders, and (C; right) the difference between the two. Parameter values used in these simulations are as listed in Table 1. Flow direction is left to right in all cases. The locations of features discussed in the text (outer-bank pool, OBP; point bar, PB) are highlighted.

and (ii) analogous two-stage river channels (compound channels) that during flooding exhibit reversal of secondary flow cells at bend apices (Wormleaton et al., 2004, 2005). These experiments showed low transverse slopes at bend apices, increasing around the bend, and 'point bars' located downstream of the bend apex (Wormleaton et al., 2004, 2005; Peakall et al., 2007a; Amos et al., 2010). Direct comparison with other submarine channels is difficult because of restricted bathymetric resolution in most modern examples, and the difficulty of accurately reconstructing original point-bar positions and extent relative to bend apices from 'scroll bars' observed in some seismic examples (e.g., Kolla et al., 2001; Abreu et al., 2003). However, purported point bars on the Bengal Fan exhibit deposition dominantly downstream of bend apices (Schwenk et al., 2003). Depth-averaged numerical modelling of depositional flows has also suggested that the transverse slopes of submarine channels are much lower than in river channels (Das et al., 2004), as shown in this study. However, Das et al.'s (2004) model predicts that transverse slopes are greatest at bend apices, and that point bars are dominantly located upstream of bend apices. Differences between results from this study and Das et al. (2004) may be related to the neglect of bed load transport in the latter. In summary, the agreement between the model used in this study, physical modelling, and limited data from modern and ancient submarine channels, suggests that 'point bars' in submarine channels exhibiting reversed secondary flow may indeed be located further downstream relative to bend apices than those in meandering river channels.

The simulations presented in this paper focus on the morphological impacts of the (reversed) secondary flow circulations associated with (some) turbidity currents. Nevertheless, given the strong relationship between bed morphology and surface grain-size distributions within meander bends, a number of sedimentological implications also seem likely. Specifically, as a consequence of the relative downstream migration of 'point bars' and reduced transverse slopes: (i) patterns of grain-size sorting and consequently facies should vary relative to fluvial channels with point bars showing up to an order of magnitude thinner fining-up sequences for a given channel depth than in comparable meandering river channels (cf., Dykstra and Kneller, 2009; Pyles et al., 2010), and an absence or greatly restricted presence of coarsening-up sequences as observed in the upstream parts of fluvial point bars (Jackson, 1976; Willis, 1989; Peakall et al., 2007b); (ii) bend apices should display only very limited lateral grain-size variations (Bridge, 1992; Wormleaton et al., 2005); (iii) the depth of outer-bank scour and therefore the thickness of localised coarse-grained deposits may be restricted relative to rivers, and; (iv) the growth of 'point bars' that are shifted downstream relative to bend apices should lead to preferential migration of the downstream limbs of bends with a resulting increase in bend asymmetry, and preservation of deposits that may exhibit a planform expression analogous to concave benches in river channels (cf. Abreu et al., 2003).

5. Conclusion

In this paper a model of bed topography for submarine meander bends has been developed by modifying Bridge's (1992) model of bend morphology in fluvial meanders. This was achieved by replacing the vertical profile of downstream flow velocity with a function valid for gravity currents. Resulting transverse velocities were characterised by secondary flow cells with a reversed orientation relative to river channels. The modified model was used to replicate transverse bed gradients at the apices of eleven individual bends within (i) a large, presently inactive, submarine meandering system in the Gulf of Alaska, (ii) an active submarine meander bend in the Black Sea, and; (iii) experimental submarine meander channels modelled in the laboratory. In the cases of the Black Sea and experimental bends, the secondary flow circulations are known to exhibit reversed helicity, while reconstruction of flows through the Gulf of Alaska meanders suggests that the majority of these bends would also have exhibited reversed secondary flow circulations. The submarine meanders simulated in this study exhibit key differences in bed morphology relative to equivalent fluvial bends. Specifically, the outer-bank pools are shallower and point bars are less pronounced, resulting in a

transverse bed profile gradient that is much flatter than is typical in fluvial bends. In addition, results of simulations for a single hypothetical meander bend indicate that the position of the point bar is located further downstream of the bend apex than is normally the case in fluvial meanders.

In contrast to the mechanism of secondary flow reversal that is the focus of the present study, Islam and Imran (2008) have suggested that point-bar suppression could also be induced in instances where the secondary flow structure of density driven gravity underflows consists of two (not one as suggested by Corney et al. (2006, 2008) and Keevil et al. (2006, 2007) and reproduced herein) secondary flow cells stacked on top of each other. These twin cells result from either curvature induced flow splitting or downstream velocity profiles with the velocity maximum located far from the bed (Islam and Imran, 2008; Islam et al., 2008). In such cases the near-bed cell has the same rotation as the classic secondary flow cell for fluvial meanders, whereas it is the upper cell that has the reversed sense of rotation employed herein. Islam and Imran (2008) suggest that it is the restricted vertical extent of the near-bed cell, this extent being limited by the height above the bed of the downstream flow velocity maximum, which acts to limit point-bar deposition and outer-bank scour relative to a terrestrial river under otherwise similar conditions. It is likely that different submarine meander systems, subject to different controlling factors such as bend geometry and cross-section shape, have different secondary flow structures, but interestingly these differing flow mechanisms may in fact converge to give very similar vertical topographic expression of meander bend morphology; though different secondary flows will lead to spatial changes in point-bar position.

Further research is clearly required to (i) test the extent to which these findings can be transferred to other submarine meanders, (ii) more clearly discriminate the conditions under which different secondary flow structures emerge, and (iii) evaluate if dissimilar secondary flow structures result in the production of similar topographic outcomes. While much remains to be learned, there is a growing body of evidence to suggest that models of submarine meanders developed by analogy with fluvial meanders are not correct. This has particularly significant implications in the context of seeking to understand facies patterns and spatial variations in grain-size sorting, and bend evolution dynamics within these submarine channel systems.

Acknowledgements

We thank Kathryn Amos, Gareth Keevil and Dan Parsons for the assistance with calculating the parameters for Table 1, and Julian Leyland for assistance with morphometric analysis of the Gulf of Alaska meanders. We greatly appreciate the perceptive comments made by the two anonymous reviewers; their suggestions helped us to significantly improve the quality of the final manuscript.

References

Abad, J.D., Sequeiros, O., Spinewine, B., Pirmez, C., Garcia, M.H., Parker, G., 2011. Secondary current of saline underflow in a highly meandering channel: Experiments, theory, field. Journal of Sedimentary Research 81, 787–813.

Abreu, V., Sullivan, M., Pirmez, C., Mohrig, D., 2003. Lateral accretion packages (LAP's): an important reservoir element in deep water sinuous channels. Marine and Petroleum Geology 20, 631–648.

Altinakar, M.S., Graf, W.H., Hopfinger, E.J., 1996. Flow structure in turbidity currents. Journal of Hydraulic Research 34, 713–718.

Amos, K.J., Peakall, J., Bradbury, P.W., Roberts, M., Keevil, G., Gupta, S., 2010. The influence of bend amplitude and planform morphology on flow and sedimentation in submarine channels. Marine and Petroleum Geology 27, 1431–1447. doi:10.1016/j.marpetgeo.2010.05.004.

Babonneau, N., Savoye, B., Cremer, M., Klein, B., 2002. Morphology and architecture of the present canyon and channel system off the Zaire deep-sea fan. Marine and Petroleum Geology 19, 445–467.

Best, J.L., Ashworth, P.J., 1994. A high resolution ultrasonic bed profiler for use in laboratory flumes. Journal of Sedimentary Research A64, 674–675.

Best, J.L., Kirkbride, A.D., Peakall, J., 2001. Mean flow and turbulence structure of sediment-laden gravity currents: new insights using ultrasonic Doppler velocity profiling. In: McCaffrey, W.D., Kneller, B.C., Peakall, J. (Eds.), Particulate Gravity Currents, International Association of Sedimentologists Special Publication, 31, pp. 159–172.

Bouma, A.H., Coleman, J.M., DSDP Leg 96 Shipboard Scientists, Bouma, A.H., Normark, W.R., Barnes, N.E., 1985. Mississippi Fan: Leg 96 program and principal results. Submarine Fans and Related Turbidite Systems. Springer, New York, pp. 247–252.

Bridge, J.S., 1992. A revised model for water flow, sediment transport, bed topography and grain size sorting in natural river bends. Water Resources Research 28, 999–1013.

Bridge, J.S., Bennett, S.J., 1992. A model for the entrainment and transport of sediment grains of mixed sizes, shapes and densities. Water Resources Research 28, 337–363.

Buckee, C., Kneller, B., Peakall, J., 2001. Turbulence structure in steady solute-driven gravity currents. In: McCaffrey, W.D., Kneller, B.C., Peakall, J. (Eds.), *Particulate Gravity Currents*, International Association of Sedimentologists, Special Publication, 31, pp. 173–188.

Clark, J.D., Pickering, K.T., 1996. Submarine Channels: Processes and Architecture. Vallis Press, London. 231 pp.

Corney, R.K.T., Peakall, J., Parsons, D.R., Elliott, L., Amos, K.J., Best, J.L., Keevil, G.M., Ingham, D.B., 2006. The orientation of helical flow in curved channels. Sedimentology 53, 249–257.

Corney, R.K.T., Peakall, J., Parsons, D.R., Elliott, L., Best, J.L., Thomas, R.E., Keevil, G.M., Ingham, D.B., Amos, K.J., 2008. Reply to discussion of Imran et al. on "The orientation of helical flow in curved channels" by Corney et al., Sedimentology, 53, 249–257. Sedimentology 55, 241–247.

Curray, J.R., Emmel, F.J., Moore, D.G., 2003. The Bengal Fan: morphology, geometry, stratigraphy, history and processes. Marine and Petroleum Geology 19, 1191–1223.

Damuth, J.E., Flood, R.D., 1984. Morphology, sedimentation processes, and growth pattern of the Amazon deep-sea fan. Geo-Marine Letters 3, 109–117.

Darby, S.E., Delbono, I., 2002. A model of equilibrium bed topography for meander bends with erodible banks. Earth Surface Processes and Landforms 27, 1057–1085.

Das, H.S., Imran, J., Pirmez, C., Mohrig, D., 2004. Numerical modeling of flow and bed evolution in meandering submarine channels. Journal of Geophysical Research 109, C10009. doi:10.1029/2002JC001518.

Dietrich, W.E., 1982. Settling velocities of natural particles. Water Resources Research 18, 1615–1626.

Droz, L., Rigaut, F., Cochonat, P., Tofani, R., 1996. Morphology and recent evolution of the Zaire turbidite system (Gulf of Guinea). Geological Society of America Bulletin 108, 253–269.

Dykstra, M., Kneller, B., 2009. Lateral accretion in a deep-marine channel complex: implications for channellized flow processes in turbidity currents. Sedimentology 56, 1411–1432. doi:10.1111/j.1365-3091.2008.01040.x.

Engelund, F., 1974. Flow and bed topography in channel bends. Journal of the Hydraulics Division of the American Society of Civil Engineers 100, 1631–1648.

Felix, M., 2002. Flow structure of turbidity currents. Sedimentology 49, 397–419.

Felix, M., 2004. The significance of single value variables in turbidity currents. Journal of Hydraulic Research 42, 323–330.

Flood, R.D., Hiscott, R.N., Aksu, A.E., 2009. Morphology and evolution of an anastomosed channel network where saline underflow enters the Black Sea. Sedimentology 56, 807–839.

Garcia, M., Parker, G., 1993. Experiments on the entrainment of sediment into suspension by a dense bottom current. Journal of Geophysical Research 98, 4793–4807.

Giorgio Serchi, F., Peakall, J., Ingham, D.B., Burns, A.D., 2011. A unifying computational fluid dynamics investigation on the river-like to river-reversed secondary circulation in submarine channel bends, Journal of Geophysical Research 116, C06012. doi:10.1029/2010JC006361.

Imran, J., Islam, M.A., Huang, H., Kassem, A., Dickerson, J., Pirmez, C., Parker, G., 2007. Helical flow couplets in submarine gravity underflows. Geology 35, 659–662.

Islam, M.A., Imran, J., 2008. Experimental modeling of gravity underflow in a sinuous submerged channel. Journal of Geophysical Research 113, C07041. doi:10.1029/2007JC004292.

Islam, M.A., Imran, J., Pirmez, C., Cantelli, A., 2008. Flow splitting modifies the helical motion in submarine channels. Geophysical Research Letters 35, L22603. doi:10.1029/2008GL034995.

Jackson, R.G., 1976. Depositional model of point bars in the Lower Wabash River. Journal of Sedimentary Petrology 46, 579–594.

Keevil, G.M., Peakall, J., Best, J.L., Amos, K.J., 2006. Flow structure in sinuous submarine channels: velocity and turbulence structure of an experimental submarine channel. Marine Geology 229, 241–257.

Keevil, G.M., Peakall, J., Best, J.L., 2007. The influence of scale, slope and channel geometry on the flow dynamics of submarine channels. Marine and Petroleum Geology 24, 487–503.

Kenyon, N.H., Amir, A., Cramp, A., 1995. Geometry of the younger sediment bodies of the Indus Fan. In: Pickering, K.T., Hiscott, R.N., Kenyon, N.H., Lucchi, F.R., Smith, R.D.A. (Eds.), Atlas of Deepwater Environments: Architectural Styles in Turbidite Systems. Chapman & Hall, London, pp. 89–93.

Khripounoff, A., Vangriesheim, A., Babonneau, N., Crassous, P., Dennielou, B., Savoye, B., 2003. Direct observation of intense turbidity current activity in the Zaire submarine valley at 4000 m water depth. Marine Geology 194, 151–158.

Kikkawa, H., Ikeda, S., Kitagawa, A., 1976. Flow and bed topography in curved open channels. Journal of the Hydraulics Division of the American Society of Civil Engineers 102 (HY9), 1327–1342.

Klaucke, I., Hesse, R., 1996. Fluvial features in the deep-sea: new insights from the glacigenic submarine drainage system of the Northwest Atlantic Mid-Ocean Channel in the Labrador Sea. Sedimentary Geology 106, 223–234.

Kneller, B., 2003. The influence of flow parameters on turbidite slope channel architecture. Marine and Petroleum Geology 20, 901–910.
Kolla, V., Bourges, P., Urrity, J.M., Safa, P., 2001. Evolution of deepwater Tertiary sinuous channels offshore Angola (west Africa) and implications for reservoir architecture. Bulletin of the American Association of Petroleum Geologists 85, 1373–1405.
Komar, P.D., 1969. The channelized flow of turbidity currents with application to Monterey Deep-Sea Channel. Geological Society of America Bulletin 78, 4544–4558.
Mayer, L.M., Gardner, J.V., Armstrong, A., Calder, B.R., Malik, M., Angwenyi, C., Karlpata, S., Montoro-Dantes, H., Morishita, T., Mustapha, A., Van Waes, M., Wood, D., Withers, A., 2005. New views of the Gulf of Alaska margin mapped for UNCLOS applications. Eos Transactions of the American Geophysical Union 86 (52) Fall Meeting Supplement, Abstract T13D-0500.
Özsoy, E., Latif, M.A., Tuğrul, S., Ünlülata, Ü., 1995. Exchanges with the Mediterranean, fluxes and boundary mixing processes in the Black Sea. In: Briand, F. (Ed.), Mediterranean Tributary Seas. : Spec. Publ. 15, CIESME Science Series, vol. 1. Bulletin de l'Institut Océanographique, Monaco, pp. 1–25.
Özsoy, E., Di Iorio, D., Gregg, M., Backhaus, J.O., 2001. Mixing in the Bosphorus Strait and the Black Sea continental shelf: observations and a model of the dense water outflow. Journal of Marine Systems 31, 99–135.
Parker, G., Andrews, E.D., 1985. Sorting of bed load sediments by flow in meander bends. Water Resources Research 21, 1361–1373.
Parsons, D.R., Peakall, J., Aksu, A.E., Flood, R.D., Hiscott, R.N., Beşiktepe, Ş., Mouland, D., 2010. Gravity-driven flows in a submarine channel bend: direct field evidence of helical flow reversal. Geology 38, 1063–1066. doi:10.1130/G31121.1.
Paull, C.K., Ussler, W., Greene, H.G., Keaten, R., Mitts, P., Barry, J., 2003. Caught in the act: the 20 December 2001 gravity flow event in Monterey Canyon. Geo-Marine Letters 22, 227–232.
Peakall, J., Amos, K.J., Keevil, G.M., Bradbury, P.W., Gupta, S., 2007a. Flow processes and sedimentation in submarine channel bends. Marine and Petroleum Geology 24, 470–486.
Peakall, J., Ashworth, P.J., Best, J.L., 2007b. Meander-bend evolution, alluvial architecture, and the role of cohesion in sinuous river channels: a flume study. Journal of Sedimentary Research 77, 197–212. doi:10.2110/jsr.2007.017.
Pirmez, C., Imran, J., 2003. Reconstruction of turbidity currents in Amazon Channel. Marine and Petroleum Geology 20, 823–849.
Pyles, D., Jennette, D.C., Tomasso, M., Beaubouef, R.T., Rossen, C., 2010. Concepts learned from a 3D outcrop of a sinuous slope channel complex: Beacon Channel complex, Brushy Canyon Formation, west Texas. Journal of Sedimentary Research 80, 67–96.
Schwenk, T., Spieß, V., Hübscher, C., Breitzke, M., 2003. Frequent channel avulsions within the active channel-levee system of the middle Bengal Fan — an exceptional channel-levee development derived from Parasound and Hydrosweep data. Deep-sea Research Part II 50, 1023–1045.
Sequeiros, O.E., Spinewine, B., Beaubouef, R.T., Sun, T., Garcia, M.H., Parker, G., 2010. Characteristics of velocity and excess density profiles of saline underflows and turbidity currents flowing over a mobile bed. Journal of Hydraulic Engineering 136 (7), 412–433.
Stacey, M.W., Bowen, A.J., 1988. The vertical structure of density and turbidity currents: theory and observations. Journal of Geophysical Research 93, 3528–3542.
Straub, K.M., Mohrig, D., McElroy, B., Buttles, J., 2008. Interactions between turbidity currents and topography in aggrading sinuous submarine channels: a laboratory study. GSA Bulletin 120, 368–385.
Tesaker, E., 1969. Uniform turbidity currents, Unpublished doctoral thesis, Technical University of Norway, Trondheim.
Vangriesheim, A., Khripounoff, A., Crassous, P., 2009. Turbidity events observed in situ along the Congo Submarine Channel. Deep Sea Research II 56, 2208–2222.
Willis, B.J., 1989. Palaeo-channel reconstructions from point bar deposits: a three dimensional perspective. Sedimentology 36, 757–766.
Wormleaton, P.R., Sellin, R.H.J., Bryant, T., Loveless, J.H., Hey, R.D., Catmur, S.E., 2004. Flow structures in a two-stage channel with a mobile bed. Journal of Hydraulic Research 42, 145–162.
Wormleaton, P.R., Hey, R.D., Sellin, R.H.J., Bryant, T., Loveless, J., Catmur, S.E., 2005. Behavior of meandering overbank channels with graded sand beds. Journal of Hydraulic Engineering 131, 665–681.
Wynn, R.B., Cronin, B.T., Peakall, J., 2007. Sinuous deep-water channels: genesis, geometry and architecture. Marine and Petroleum Geology 24, 341–387.
Xu, J.P., 2010. Normalized velocity profiles of field-measured turbidity currents. Geology 38 (6), 563–566. doi:10.1130/G30582.1.
Xu, J.P., Noble, M.A., Rosenfeld, L.K., 2004. In-situ measurements of velocity structure within turbidity currents. Geophysical Research Letters 31, L09311. doi:10.1029/2004GL019718.